Published in final edited form as:
*Biomaterials*. 2015 January ; 36: 124–133. doi:10.1016/j.biomaterials.2014.09.017.

# Self-assembled Nanoscale Coordination Polymers Carrying siRNAs and Cisplatin for Effective Treatment of Resistant Ovarian Cancer

**Chunbai He**, **Demin Liu**, and **Wenbin Lin***
Department of Chemistry, University of Chicago, 929 E 57th St, Chicago, IL 60637, USA

## Abstract

Resistance to the chemotherapeutic agent cisplatin is a major limitation for the successful treatment of many cancers. Development of novel strategies to overcome intrinsic and acquired resistance to chemotherapy is of critical importance to effective treatment of ovarian cancer and other types of cancers. We have sought to re-sensitize resistant ovarian cancer cells to chemotherapy by co-delivering chemotherapeutics and pooled siRNAs targeting multi-drug resistance (MDR) genes using self-assembled nanoscale coordination polymers (NCPs). In this work, NCP-1 particles with trigger release properties were first constructed by linking cisplatin prodrug-based bisphosphonate bridging ligands with $Zn^{2+}$ metal-connecting points and then coated with a cationic lipid layer, followed by the adsorption of pooled siRNAs targeting three MDR genes including survivin, Bcl-2, and P-glycoprotein via electrostatic interactions. The resulting NCP-1/siRNA particles promoted cellular uptake of cisplatin and siRNA and enabled efficient endosomal escape in cisplatin-resistant ovarian cancer cells. By down-regulating the expression of MDR genes, NCP-1/siRNAs enhanced the chemotherapeutic efficacy as indicated by cell viability assay, DNA ladder, and flow cytometry. Local administration of NCP-1/siRNAs effectively reduced tumor sizes of cisplatin-resistant SKOV-3 subcutaneous xenografts. This work shows that the NCP-1/siRNA platform holds great promise in enhancing chemotherapeutic efficacy for the effective treatment of drug-resistant cancers.

### Keywords

nanoscale coordination polymers; siRNA; cisplatin; overcome drug-resistance; ovarian cancer treatment

## 1. Introduction

Ovarian cancer is the fifth most prevalent cancer among women in the United States, with a lifetime risk of 1.4%–1.8%. Development of multi-drug resistance (MDR) in ovarian cancer



***Corresponding author:** Tel: (+) 1 773 834 7163; Fax: (+) 1 773 702 0805, wenbinlin@uchicago.edu.

cells is one of the major obstacles for effective chemotherapy [1–4]. After repeated treatment with anticancer chemotherapeutic agents, tumor cells develop strategies to increase their resistance to chemotherapy to avoid programmed death by activating anti-apoptotic pathways [5–10]. Although a combination of chemotherapeutic agents are often used to prevent drug resistance in cancer patients, the ability of the cancer cells to adapt and develop one or more drug resistance pathways ultimately leads to failure in the treatment of ovarian and other cancers [11, 12]. In ovarian cancer, the majority of patients (50–75%) have recurrent and incurable cancer after their successful initial treatment with platinum drug or paclitaxel [13]. The development of therapeutic strategies to overcome drug resistance will have a great impact on the treatment of ovarian cancer.

Small interfering RNA (siRNA) has the ability to disrupt cellular MDR pathways by silencing relevant gene expressions, opening the door for re-sensitizing the cancer cells which have acquired resistance to anticancer drugs [14, 15]. However, drug resistance often involves multiple and dynamically acquired MDR mechanisms as a result of the overexpression of drug efflux pumps (e.g., P-glycoprotein, P-gp or MDR1); multidrug resistance protein, MRP, anti-apoptotic proteins (e.g., Bcl-2, survivin), oncogenes (e.g., c-Myc), and regulators of drug metabolism (e.g., pregnane X receptor, PXR) [16–21]. P-gp is overexpressed in the malignant tissues and becomes an attractive target to overcome MDR [16, 22]. Bcl-2 is responsible for the activation of cellular anti- apoptotic defense [23]. Survivin has a functional role in caspase inhibition to lead to negative regulation of apoptosis, and is upregulated in most human tumors, making it a potential target for cancer treatment [17, 24]. We hypothesized that delivering pooled siRNAs, including siP-gp, siBcl-2, and sisurvivin, targeting different molecular signaling pathways would be an effective approach to overcoming drug resistance in cancers.

Nanoparticulate delivery systems have been shown to improve therapeutic efficacy of anticancer chemotherapeutics by enhancing drug delivery to tumors and thereby reducing general toxicity through the enhanced permeability and retention (EPR) effect [25–33]. However, free nucleic acid drugs, such as siRNAs, cannot be used for cancer treatment in vivo due to their ready degradation by nucleases. Nanoparticles have been shown to provide protection to siRNAs and mediate efficient gene silencing in cancer cells [24, 34–39]. Co-delivery of anticancer chemotherapeutics and siRNAs targeting MDR genes in the same nanoparticle can drastically enhance therapeutic efficacy by overcoming drug resistance in cancer cells. Several nanoparticle systems, including liposomes, carbon nanotubes, and polymer micelles, have recently been used to co-deliver siRNA and cisplatin to cancer cells both in vitro and in vivo in order to enhance therapeutic responses [40–42].

Herein we report a novel self-assembled nanoscale coordination polymer (NCP) system for the co-delivery of cisplatin and pooled siRNAs to cisplatin-resistant ovarian cancer cells (ES-2, OVCAR-3, SKOV-3, and A2780/CDDP cells) to overcome drug resistance by re-sensitizing the cells to cisplatin treatment. NCPs are self-assembled from metal ions and organic bridging ligands, which have numerous advantages over conventional drug delivery systems such as high drug loadings, tunable compositions, shapes, and sizes, and readily modifiable surface [43]. Our group has developed a series of NCPs as potential delivery systems for chemotherapeutics [44–48]. In particular, we recently reported the self-assembly

of zinc bisphosphonate NCPs that contain 48 wt% cisplatin prodrug by linking the cisplatin prodrug cis,cis,trans-[$Pt(NH3)_2Cl_2(OCONHP(O)(OH)_2)_2$] with $Zn^{2+}$ ions.[43] Upon pegylation with the 1,2-dioleoyl-sn-glycero-3-phosphocholine (DOPC)/cholesterol/1,2-distearoyl-sn-glycero-3-phosphoethanolamine-N-[amino(polyethylene glycol)-2000] (DSPE-PEG2k) coating, these NCPs showed much enhanced stability in the blood circulation and possessed superior anticancer efficacy in multiple non-resistant murine tumor xenograft models compared to free drugs [43]. In this study, we used cationic lipid 1,2-dioleoyl-3-trimethylammonium-propane (DOTAP) instead of DOPC to coat NCP-1 to yield positively charged particles which strongly bind to negatively charged siRNAs via electrostatic interactions to afford siRNA-encapsulated NCP-1 particles (NCP-1/siRNAs) (Scheme 1). We examined siRNA protection, siRNA release profiles, and cell uptake and MDR gene silencing efficiency of NCP-1/siRNAs in ovarian cancer cells. We evaluated the in vitro anticancer effect of NCP-1/siRNAs by cell viability assay, DNA ladder, Annexin V staining, and flow cytometry in cisplatin-resistant ovarian cancer cells. Finally, we demonstrated the significantly enhanced chemotherapeutic efficacy of NCP-1/siRNAs in SKOV-3 tumor bearing mice.

## 2. Materials and methods

### 2.1. Materials, cell lines, and animals

All of the starting materials were purchased from Sigma-Aldrich and Fisher (USA), unless otherwise noted, and used without further purification. 1,2-dioleoyl-sn-glycero-3-phosphate (DOPA), 1,2-dioleoyl-3-trimethylammonium-propane (DOTAP), cholesterol , and 1,2-distearoyl-sn-glycero-3-phosphoethanolamine-N-[amino(polyethylene glycol)2000] (DSPE-PEG2k) were purchased from Avanti Polar Lipids (USA). The siRNA duplexes were supplied by Dharmacon (USA) and dissolved in diethylpyrocarbonate (DEPC)-treated water before use. Survivin siRNA (*sisurvivin*), Bcl-2 siRNA (*siBcl-2*), and P-gp siRNA (*siP-gp*) contained the anti-sense sequences of 5’-GGACCACCGCAUCUCUACAdTdT-3’, 5’-UUCGGCAUUAGGCCUUCCGdTdG-3’, and 5’-AGCTTATAATGGATGTACT-3’, respectively. TAMRA-labeled survivin siRNA was bought from Dharmacon (USA) and used for quantification and confocal laser scanning microscopy (CLSM).

Three kinds of human ovarian cancer cells, ES-2, OVCAR-3, and SKOV-3 cells and murine macrophage Raw 264.7 cells were from the American Type Culture Collection (Rockville, MD, USA). ES-2 and SKOV-3 cells were cultured in McCoy's 5a medium containing 10% fetal bovine serum (FBS). OVCAR-3 cells were cultured in RPMI-1640 medium (Gibco, Grand Island, NY, USA) containing 10% FBS. Raw 264.7 cells were cultured in DMEM medium containing 10% FBS. Cisplatin-sensitive and -resistant human ovarian cancer cells A2780 and A2780/CDDP were obtained from Developmental Therapeutics Core, Northwestern University and were cultured in RPMI 1640 containing 10% FBS.

Athymic female nude mice (8 weeks, 20–25 g) were provided by Harlan Laboratories, Inc. (USA). The study protocol was reviewed and approved by the Institutional Animal Care and Use Committee (IACUC) at the University of Chicago.

### 2.2. Preparation and characterization of NCP-1/siRNAs

NCP-1 nanoparticles were prepared according to our previous report with modifications [43]. Briefly, the cisplatin prodrug, cis,cis,trans- $[Pt(NH_3)_2Cl_2(OCONHP(O)(OH)_2)_2]$, was synthesized following our previous procedures [43]. Two hundred microliters of 25 mg/mL cisplatin prodrug solution and 0.2 mL of 100 mg/mL $Zn(NO_3)_2$ aqueous solution were added to 5 mL of 0.3 M Triton X-100/1.5 M 1-hexanol in cyclohexane mixture, respectively, to form w = 7.4 microemulsions. Two hundred microliter of DOPA (200 mg/mL in $CHCl_3$) was added to the cisplatin prodrug microemulsion and the stirring was continued for 15 min until a clear solution formed. The two microemulsions were combined, and the resultant 10 mL of microemulsion was stirred for 30 additional minutes to yield DOPA-coated NCP particles, which were then washed with cyclohexane and ethanol to remove excess DOPA, and dispersed in THF.

The cationic lipid coated NCP-1 was prepared by adding a THF solution of DOTAP, cholesterol (molar ratio of DOTAP/cholesterol = 2:1), 20 mol% DSPE-PEG2k, and DOPA-coated NCP to 30% (v/v) ethanol/water at 50 °C. THF and ethanol were completely evaporated and the NCP-1 solution was allowed to cool down to room temperature. The NCP-1 was centrifuged at 13000 rpm for 30 min followed by the removal of the supernatant and re-suspending the nanoparticle precipitate in DEPC-treated water.

The control nanoparticles (Zn control) were prepared with the same method except that sodium pyrophosphate decahydrate was used instead of cisplatin prodrug to form the NCPs. sisurvivin, siBcl-2, and siP-gp were dissolved in DEPC-treated water at weight ratio of 1: 1: 1 to achieve 2 mg/mL pooled siRNA solution. Cationic lipid coated NCP-1 (2 mg/mL) was mixed with siRNA solution (2 mg/mL) at weight ratio of cisplatin:siRNA=4:1, and the mixture was stirred at 800 rpm and at room temperature for 30 min to allow the adsorption of negatively charged siRNA onto positively charged NCP-1 surface.

Inductively coupled plasma-mass spectrometry (ICP-MS, Agilent Technologies, USA) was utilized to analyze the Pt concentration of NCP to calculate the cisplatin loading efficiency. The particle size and Zeta potential of NCP-1 and NCP-1/siRNAs in phosphate buffered solution (PBS) were determined with Zetasizer (Nano ZS, Malvern, UK). Transmission electron micrsocopy (TEM, JEM 100CX-II, JOEL, Japan) was used to observe the morphology of NCP-1 and NCP-1/siRNAs.

The *in vitro* stability of NCP-1/siRNAs in terms of particle size and polydispersity index (PDI) was evaluated in phosphate buffer saline (PBS) supplemented with 5 mg/mL bovin serum albumin (BSA). NCP-1/siRNA (1 mg/mL) was incubated with PBS containing 5 mg/mL BSA at 37 °C for 12 h, and the particle size and PDI were monitored during the 12-h incubation by DLS.

The association of siRNA with NCP-1 was first determined with gel retardation assay on 4% (w/v) agarose gel electrophoresis containing 0.25 μg/mL of EB. We also quantitatively determined the encapsulation efficiency (EE) of siRNA onto NCP-1 by fluorimetry. TAMRA-labeled siRNA was encapsulated into NCP-1 and the nanoparticle suspension was centrifuged at 13,000 rpm for 30 min. The amount of free TAMRA-siRNA in the

supernatant was determined with fluorimetry based on the standard curve (TAMRA, $\lambda_{ex}$ = 565 nm, $\lambda_{em}$ = 580 nm). EE was calculated from the following equation:

$$EE(\%) = \frac{W_0 - W_1}{W_0} \times 100$$

where $W_0$ and $W_1$ stand for the content of total siRNA and free siRNA in the supernatant, respectively.

### 2.4. siRNA protection and release

NCP-1/siRNAs containing 1 μg of siRNA was mixed with equal volume of FBS. After incubation at 37 °C for a pre-determined time, the mixture was heated at 80 °C for 5 min to inactivate the nucleases and disrupt the NCP-1 structure. Thus, the siRNA was dissociated from NCP-1/siRNA, and its integrity was subsequently evaluated on 4% (w/v) agarose gel electrophoresis. A free siRNA solution containing 1 μg of siRNA served as control. Image J was used to quantify the intensity of each siRNA migration band in order to give the quantitative siRNA degradation curve. The intensity of the band representing siRNA control (containing 1 μg of siRNA) served as 100% intensity.

As for the evaluation of siRNA release profiles from NCP-1/siRNAs, nanoparticles containing 1 μg of TAMRA-siRNA were incubated with 1 mL of PBS at 37 °C with shaking. At pre-determined time intervals, the suspension was centrifuged at 13,000 rpm for 10 min and 0.5 mL of the supernatant was quantified for the TAMRA-siRNA content by fluorimetry. An equal volume of the release medium was added, and the precipitate was re-suspended before further incubation.

### 2.5. Cisplatin release

The release profiles of cisplatin from the lipid coated NCP-1 and NCP-1/siRNAs were investigated. The release profiles were performed in 400 mL of 6.7 mM PBS buffer at 37°C. The NCP-1 (3 mg) was suspended in 5 mL of 6.7 mM PBS buffer in a 10,000 MWCO pleated dialysis bag. The dialysis bag containing nanoparticle suspension was then put in the beaker followed by the addition of 400 mL of 5 mM PBS buffer, and the system was incubated at 37 °C under stirring. Periodically, 1 mL aliquots of the solution were removed, and 1 mL of fresh buffer solution was added to the beaker. The removed aliquots were collected and analyzed by ICP-MS for Pt content. For the experiments carried out under reducing environments, 6.7 mM PBS supplemented with 5mM cysteine was used for the release profiles.

### 2.6. Cellular uptake and endosomal escape

Three kinds of ovarian cancer cell lines including ES-2, OVCAR-3, and SKOV-3 cells were seeded on a 24-well plate at $1\times10^5$ cells per well and cultured for 24 h. TAMRA-siRNA-containing NCP-1/siRNA and free TAMRA-siRNA solution (2 mg/mL) were added (0.4 μg siRNA/well). Following a 4-h incubation, cells were washed with PBS three times and then lysed with 0.5% (w/v) sodium dodecyl sulfate (SDS, pH 8.0). The lysate was quantified for TAMRA-siRNA by fluorimetry and protein content by the BCA kit (Promega, USA).

Uptake level was expressed as the amount of TAMRA-siRNA associated with 1 mg of cellular protein.

In order to determine the amount of Pt internalized by the SKOV-3 cells, the cells were collected and centrifuged at 3000 rpm 5 min after incubating with free cisplatin, NCP-1, and NCP-1/siRNAs for 4 h or 24 h, respectively. The empty centrifuge tubes were first weighed and their weights were recorded as $W_1$. The cell suspension was added to the tubes followed by centrifugation. The supernatant was discarded and the cell pellet in the tubes was completely dried. Then the tubes containing cell pellet were weighed again and their weights were recorded as $W_2$. The weight of the cell pellet was obtained by subtracting $W_1$ from $W_2$. The cell pellets were then digested in concentrated nitric acid for 24 h. The amount of internalized Pt was determined by ICP-MS.

A time dependent study of endosomal escape was performed by incubating NCP-1/siRNAs with SKOV-3 cells for 10, 30, 60, 90, and 120 min followed by Lysotracker Green (100 nM) and DAPI (10 μg/mL) staining. The time-dependent co-localization of NCP-1/siRNAs and endosome/lysosome was observed under CLSM (Olympus FV1000, Japan), and the co-localization efficiency was quantitatively determined using Image J (co-localization threshold) based on the CLSM images.

### 2.7. In vitro gene silencing

ES-2, OVCAR-3, and SKOV-3 cells were seeded at $2\times10^5$ cells per well in 24-well plates and further cultured for 24 h. The culture media were replaced by 1 mL of pre-warmed and fresh culture media containing 10% fetal bovine serum (FBS) prior to the experiment. NCP-1/siRNAs, NCP-1/si*Bcl-2*, NCP-1/si*P-gp*, NCP-1/si*survivin*, Zn control/siRNAs, and NCP-1 were added to the cells at a siRNA dose of 30 nM, corresponding to the cisplatin dose of 1.6 μg per well. Following incubation for 4 h, the culture media were replaced by pre-warmed and fresh culture media containing 10% FBS, and additional 20 h of incubation was allowed. The supernatant of the culture media was collected for the determination of extracellular survivin and P-gp production by ELISA (R&D Systems, USA; MyBiosource, USA) following manufacturer's instructions. The cells were lysed, and the Bcl-2 amount in the lysate was quantified by ELISA (R&D Systems, USA). Dose-dependent in vitro transfection was carried out on SKOV-3 cells, and the gene silencing efficiency mediated by NCP-1/siRNAs was compared with commercialized transfection reagent Lipofectamine RNAiMAX (Life Technology, USA).

In addition, RNA was isolated from the transfected SKOV-3 cells according to the Trizol reagent protocol (Invitrogen, USA), and cDNA was synthesized from 500 ng of total RNA using PrimeScript ®RT reagent kit (Takara Biotechnology Co. Ltd) according to the manufacturer's instructions. Synthesized cDNA, forward and reverse primers, and the SYBR Premix Ex Taq™ (Takara Biotech. Co., Ltd.) were run on the CFX96 Real-Time PCR Detection System (Bio-Rad, USA) for the evaluation of cellular *Bcl-2, survivin, and P-gp* mRNA levels. Sequences of the primers used were designed with Primer Bank (Supporting Information Table S1). β-actin was used as an internal loading control.

### 2.8. Cytotoxicity

ES-2, OVCAR-3, and SKOV-3 cells were seeded at 5000 cells per well while A2780 and A2780/CDDP cells were seeded at 2500 cells per well in 96-well plates and further cultured for 24 h. The culture media were replaced by 100 μL of fresh culture media containing 10% FBS. Cisplatin solution, NCP-1, NCP-1/siRNAs, NCP-1/siBcl-2, NCP-1/siP-gp, NCP-1/sisurvivin, and Zn control/siRNAs were added to the cells at different cisplatin or siRNA dose. Following incubation for 72 h, the cell viability was determined by (3-(4,5-dimethylthiazol-2-yl)-5-(3-carboxymethoxyphenyl)-2-(4-sulfophenyl)-2H-tetrazolium) (MTS) assay (Promega, USA) according to manufacture instructions. The concentrations of cisplatin and siRNA required to inhibit cell growth by 50% ($IC_{50}$ values) were calculated.

### 2.9. Apoptosis

**2.9.1. DNA ladder—**ES-2, OVCAR-3, and SKOV-3 cells were seeded at $1\times10^6$ cells per well in 6-well plates and further cultured for 24 h. The culture media were replaced by 2 mL of fresh culture media containing 10% FBS. NCP-1 and NCP-1/siRNAs were added to the cells at a cisplatin concentration of $IC_{80}$. Following incubation for 24 h, total DNA of cancer cells was extracted using DNA ladder isolation kit (Invitrogen, USA) according to the manufacture instructions and examined for DNA fragmentation on a 2% (w/v) agarose gel electrophoresis at 35 V for 5 h.

**2.9.2 Annexin V staining—**Coverslips putting in the 6-well plates were seeded with ES-2, OVCAR-3, and SKOV-3 cells at the density of $1\times10^6$ cells per well. The cells were incubated at 37°C and 5% $CO_2$ for 24 h prior to nanoparticle treatment. TAMRA-siRNA loaded NCP-1/siRNAs were incubated with cells at 37°C and 5% $CO_2$ for 24 h. Then, the cells were washed with PBS, fixed with iced 4% paraformaldehyde, and stained with 10 μg/mL of DAPI and Alexa Fluor 488 conjugated Annexin V (Invitrogen, USA) according to the manufacturer's instructions. The cells were observed using confocal laser scanning microscopy (CLSM, Zeiss LSM710, German) at excitation wavelength of 405 nm, 488 nm, and 546 nm to visualize nuclei (blue fluorescence), cell apoptosis (green fluorescence) and nanoparticle internalization (red fluorescence), respectively.

**2.9.3. Flow cytometry—**SKOV-3 cells were seeded at $1\times10^6$ cells per well in 6-well plates and further cultured for 24 h. The culture media were replaced by 2 mL of fresh culture media containing 10% FBS. Free cisplatin solution, Zn control, Zn control/siRNAs, NCP-1, NCP-1/siRNAs, NCP-1/*siBcl-2*, NCP-1/*siP-gp*, and NCP-1/*sisurvivin* were added to the cells, respectively, at cisplatin concentration of 5 μM or equivalent nanoparticle concentration of 20 μg/mL. Cells incubated with saline served as control. Following incubation for 24 h, the floating and adherent cells were collected by cell scraper and stained with Alexa Fluor 488 Annexin V/dead cell apoptosis kit with Alexa Fluor 488 annexin V and PI (Invitrogen, USA) according to the manufacturer's instructions. The apoptosis was examined on a flow cytometer (LSRII Blue, BD, USA).

### 2.10. Immunogenic response

SKOV-3 cells or Raw 264.7 cells were seeded at $2\times10^5$ cells per well in 24-well plates and further cultured for 24 h. The culture media were replaced by 1 mL of fresh culture media

containing 10% FBS prior to the experiment. NCP-1 and NCP-1/siRNAs were added to the cells at a siRNA dose of 0.4 μg (30 nM) per well, corresponding to the cisplatin dose of 1.6 μg per well. Following incubation for 72 h, the supernatant of the culture media was collected for the determination of TNF-α, IL-6, and IFN-γ by ELISA (R&D Systems, USA) following manufacturer's instructions. Cells treated with saline served as controls.

### 2.11. In vivo anticancer efficacy

Tumor bearing mice were established by subcutaneous inoculation of SKOV-3 cell suspension ($5\times10^6$ cells per mouse) into the right flank region of 8-week athymic female nude mice. After the tumor volume reached approximately 100 $mm^3$, the mice were randomly divided into 5 groups (n = 6) and intratumorally injected with PBS, free cisplatin plus free pooled siRNA solution, NCP-1, Zn control/siRNAs, and NCP-1/siRNAs at equivalent cisplatin dose of 1 mg/kg and siRNA dose of 0.25 mg/kg once every week (total three injections). Tumor volumes and body weights were monitored three times every week. Tumor volumes were calculated as follows: ($width^2$ × length)/2. Finally, all mice were sacrificed 19 days after last injection, and the excised tumors were weighed.

The mRNA expression levels and protein productions of Bcl-2, P-gp, and survivin in the tumor were evaluated by Realtime-PCR and ELISA, respectively. One hundred microgram of tumor was homogenized with radioimmunoprecipitation assay buffer (RIPA buffer) and then centrifugated at 12,000 rpm for 15 min at 4 °C. The amounts of Bcl-2, P-gp, and survivin in the supernatant were measured by ELISA and normalized with total protein content determined using the BCA kit. Another 100 μg of tumor was homogenized in liquid nitrogen, and the RNA in the tumor tissues was extracted with the Trizol reagent and the intracellular Bcl-2, survivin, and P-gp mRNA levels were thereafter monitored by Realtime-PCR.

TdT-mediated dUTP nick end labeling (TUNEL) reaction was performed on 5-μm frozen tumor sections using DNA Fragmentation Detection Kit (Life Technology, USA) according to the manufacturer's instructions and observed CLSM. DNA fragment in apoptotic cells was stained with fluorescein-conjugated deoxynucleotides (green) and the nuclei were stained with DAPI (10 μg/mL). The percentage of apoptotic cells was determined by the number ratio of TUNEL-positive cells/total cells by Image J.

Blood was collected at the endpoint of in vivo antitumor efficacy experiment, and the serum was separated. The serum concentrations of TNF-α, IFN-γ, and IL-6 were detected by ELISA (R&D Systems, USA) to evaluate the immunogenic response evoked by NCP-1/siRNAs. The plasma concentration of IgE was determined by ELISA (R&D Systems, USA) to check the induction of hypersensitivity by NCP-1/siRNAs. Liver, lungs, spleen, and kidneys were also excised after the mice were sacrificed, and then fixed with formalin. Paraffin-embedded 5 μm tissue sections were stained with hematoxylin and erosin (H&E) and observed for toxicity with light microscopy.

## 3. Results and discussion

### 3.1. Synthesis and Characterization of NCP-1/siRNAs

NCP particles containing a cisplatin prodrug, cis,cis,trans-[$Pt(NH_3)_2Cl_2(OCONHP(O)(OH)_2)_2$], were synthesized according to our previous report [43], and further coated with DOTAP, cholesterol (molar ratio of DOTAP/cholesterol=2:1), and 20 mol% DSPE-PEG2k to afford cationic NCP-1. Transmission electron microscopy (TEM) images indicated the formation of spherical particles of NCP-1 coated with cationic lipid DOTAP (Figure 1a). Dynamic light scattering (DLS) measurements showed that the diameter, polydispersity index (PDI), and surface charge of NCP-1 were 134.2 ± 3.4 nm, 0.076 ± 0.013, and 16.3 ± 2.6 mV, respectively. The cisplatin loading was determined to be 25.8±2.2 wt.% by inductively coupled plasma-mass spectrometry (ICP-MS).

After complete removal of extra lipids and free liposomes by centrifugation, pooled siRNAs (si*survivin*, si*Bcl-2*, and si*P-gp*) were directly adsorbed onto the surface of NCP-1 through electrostatic interactions. *Sisurvivin*, *siBcl-2*, and *siP-gp* contained the anti-sense sequences of 5'-GGACCACCGCAUCUCUACAdTdT-3', 5'-UUCGGCAUUA-GGCCUUCCGdTdG-3', and 5'-AGCTTATAATGGATGTACT-3', respectively. Transmission electron microscopy (TEM) images showed the presence of monodisperse spherical particles of ~30 nm in diameter for NCP-1/siRNAs (Figure 1b). Particle size, PDI, and surface charge of NCP-1/siRNAs were determined to be 156.3 ± 6.7 nm, 0.087 ± 0.021, and −3.1 ± 0.5 mV, respectively, by DLS. The bigger particle size given by DLS compared to TEM is attributed to the lipid layer and siRNAs on the particle surface as well as the hydrogel nature of the NCP-1 core. The slightly increased particle size and negative charge of NCP-1/siRNAs are consistent with the successful siRNA loading. Zn control particles loaded with siRNA was synthesized under similar conditions, and their size, PDI, and surface charge were 144.2 ± 2.4 nm, 0.102 ± 0.022, and −2.9 ± 0.4 mV, respectively. NCP-1/siRNAs also exhibited enhanced stability as manifested by constant particle size and PDI in serum-containing phosphate buffer saline (PBS) over a period of 12 h (Figure S1, SI). Gel electrophoresis indicated complete capture of siRNAs by NCP-1 at a cisplatin/siRNA weight ratio of 4 (Figure S2, SI). We also quantitatively examined the siRNA encapsulation efficiency (EE) by fluorimetry. Fluorescence-labeled siRNAs was used to form NCP-1/siRNAs, and the EE was determined to be 91.2 ± 4.9%.

Successful siRNA delivery requires both sufficient protection of the cargo from nuclease degradation and its efficient release to the cell cytoplasm as a large number of intact siRNA molecules are required for mRNA recognition and RNA interference (RNAi) in the cytoplasm [49]. NCP-1/siRNAs efficiently protected siRNAs from nuclease degradation: upon incubation with serum for up to 4 h migration bands of NCP-1/siRNAs were clearly observed (Figure 1c). In contrast, the migration bands of free siRNA solution quickly faded with time due to the degradation of siRNAs. The rate of siRNA degradation was estimated by measuring the intensity of siRNA bands with Image J. After 2 h of incubation, less than 20% the free siRNA remained intact while more than 80% of siRNA was detected for NCP-1/siRNA (Figure S3, SI). After 4 h of incubation, ~12.5% of the free siRNA remained in solution while 56.2% of the siRNA loaded onto NCP-1 was detected (Figure S3, SI).

Upon loading onto the NCP-1 surface, siRNAs are likely lying flat to increase electrostatic interactions with DOTAP molecules and are shielded by DSPE-PEG2k molecules from nuclease binding and degradation [50, 51]. On the other hand, NCP-1/siRNAs effectively released siRNAs in PBS with a complete siRNA release after 24 h (Figure S4, SI), suggesting that sufficient amount of siRNA could be released into the cytoplasm once NCP-1/siRNAs were internalized by cells. The gradual release of siRNAs from the NCP-1 surface is believed to account for the slow degradation of siRNAs after incubation with serum over time. At the same time, the cisplatin could be released from the NCP-1 upon entering the cells triggered by the higher intracellular cysteine and glutathione concentrations (Figure S5, SI). After siRNA loading, the cisplatin release was slightly retarded (Figure S5, SI), which might be due to the fact that the siRNA layer further retarded the penetration of cysteine through the lipid bilayer.

### 3.2. Cellular uptake and endosomal escape

We evaluated the ability of NCP-1/siRNAs to deliver cisplatin and siRNAs to different ovarian cancer cells. Compared to the free siRNA solution, siRNA uptake of NCP-1/siRNAs was significantly enhanced (Figure 2a), indicating that NCP-1/siRNAs could assist in the siRNA internalization. The siRNA uptake was also directly observed using confocal laser scanning microscopy (CLSM). Large amounts of siRNA (red fluorescence) were located in the cytoplasm of all three ovarian cancer cell lines (Figure S6, SI). We believe that cationic DOTAP and optimal particle size of NCP-1/siRNAs were beneficial to siRNA uptake [52, 53]. The cisplatin internalization was also promoted by the NCP-1/siRNAs (Figure 2b), which might be ascribed to the decreased nanoparticle/drug efflux pump by down-regulating the P-gp expression [54].

Besides high siRNA uptake levels, successful endo/lysosomal escape is also required for efficient siRNA-mediated gene silencing. We have used CLSM to study the siRNA endosomal escape process. As shown in Fig 2d, the extent of co-localization between the siRNA fluorescence and that of lysotracker rapidly decreased over time. After a 2-h incubation, the majority of siRNA (~70%) encapsulated in the NCP-1/siRNAs has escaped from endo/lysosome compartments, as demonstrated by the steady decrease of co-localization between red fluorescence from the siRNA and green fluorescence from Lysotracker Green (that tracks endo/lysosome membranes) over the 2-h period (Figure 2c&d, Figure S7&S8, SI). The enhanced siRNA release from endo/lysosomes by NCP-1/siRNAs is likely mediated by the ion-pair formation between the positively charged groups of DOTAP and the negatively charged groups of endosome membrane. Clustered ion-pairs are known to de-stabilize both the endosome membrane and the cationic lipid coated vector [11, 55].

### 3.3. In vitro gene silencing efficiency

Upon overcoming the several barriers to gene transfection, including siRNA encapsulation, protection, release, cell internalization, and endosomal escape, NCP-1/siRNAs evoked potent gene silencing in terms of mRNA expression and protein production in ovarian cancer cells (Figure S9, SI and Figure 3) as determined by Realtime-PCR and enzyme-linked immunosorbent assays (ELISA), respectively. We compared the gene knockdown

efficiency of NCP-1/pooled siRNAs to those of NCP-1/individual siRNA in order to determine if pooled siRNAs work synergistically to downregulate the expression of relevant proteins responsible for drug resistance. Pooled siRNAs contain one-third of each individual siRNA in the NCP-1/siRNAs, with the same total siRNA dose as that of NCP-1/individual siRNA. The specific gene knockdown efficiency mediated by NCP-1 loaded pooled siRNAs and individual siRNAs as essentially identical, suggesting that pooled siRNAs likely elicit synergistic effects in silencing multiple genes. In addition, Zn control/siRNAs were also capable of down-regulating gene expression (Figure 3). The slightly decreased survivin and Bcl-2 expression levels in NCP-1 might be attributed to the cytotoxicity induced by cisplatin incorporated in the nanoparticles that influenced the expression levels of tumor growth relevant genes including *survivin* and *Bcl-2*. The gene transfection efficiency mediated by NCP-1/siRNAs was also compared with commercialized Lipofecatmine RNAiMAX (Lipo). As shown in Figure 3d–f, the gene silencing efficiency of NCP-1/siRNAs was comparable to Lipo at the recommended siRNA dose of 3 nM. When the siRNA dose was reduced to 0.75 nM, NCP-1/siRNAs was significantly more potent than Lipo. Additionally, NCP-1/siRNAs showed prolonged gene silencing with transfection efficiency of up to 50% in 3 days, suggesting their preferable stability and high potency (Figure S10, SI).

### 3.4. Cytotoxicity

To further examine whether the efficient and simultaneous suppression of survivin, Bcl-2, and P-gp can effectively increase the chemotherapy efficacy of cisplatin, the cytotoxicity of free cisplatin, NCP-1, Zn control/siRNAs, and NCP-1/siRNAs was assessed. By the co-delivery of cisplatin and pooled siRNAs, all four cisplatin-resistant ovarian cancer cell lines could be re-sensitized by NCP-1/siRNAs, as evidenced by the drastically decreased cisplatin $IC_{50}$ (the dose of a drug required for 50% inhibition) values compared to either free cisplatin or NCP-1 (Table 1, Figure S11–S13 & S15, SI).

In ES-2, OVCAR-3, SKOV-3, and A2780/CDDP cells, the cisplatin $IC_{50}$ of NCP-1/siRNAs showed a 102-, 7-, 140-, and 16-fold decrease compared to NCP-1, respectively. NCP-1/individual siRNA treatment was only slightly more potent than NCP-1 with the exception of NCP-1/si*survivin* on SKOV-3 cells (with a 21-fold decrease in $IC_{50}$ when compared to NCP-1); the $IC_{50}$ values for NCP-1/individual siRNA samples were only up to 2.6 times lower than that of NCP-1. Even the $IC_{50}$ of NCP-1/si*survivin* on SKOV-3 cells is 6.5 times higher than than of NCP-1/siRNAs. These results indicate that NCP-1/siRNAs are much more potent than NCP-1/individual siRNA, consistent with the more effective gene knockdown as discussed earlier.

In cisplatin-sensitive A2780 cell, free cisplatin, NCP-1, and NCP-1/siRNAs evoked similar cytotoxicity (Table 1, Figure S14, SI). Therefore, we believe that delivering pooled siRNAs to silence the expression of multiple MDR genes simultaneously is more effective at overcoming drug resistance than targeting a single specific gene. Importantly, NCP-1/siRNAs were able to enhance the anticancer efficacy in different types of ovarian cancer cells: ES-2 is originated from clear cell ovarian carcinoma; OVCAR-3 is from serous adenocarcinoma; SKOV-3, A2780, and A2780/CDDP are from adenocarcinoma [56].

We also evaluated the cytotoxicity of Zn control/siRNAs at the siRNA doses corresponding to cisplatin $IC_{50}$ values. No obvious differences were observed between the cell viability of Zn control/siRNAs and control (88.3±2.1%, 89.4±3.1%, 94.2±5.6%, 102.9±4.5%, and 89.4±10.2% for ES-2, OVCAR-3, SKOV-3, A2780, and A2780/CDDP, respectively), indicating that the drastically elevated anticancer efficacy of NCP-1/siRNAs results from the synergy between gene regulation by pooled siRNAs and chemotherapeutic effects of cisplatin.

### 2.5. Apoptosis

The cell apoptosis induced by NCP-1/siRNAs was analyzed by Annexin V conjugate staining, DNA ladder, and flow cytometry. As shown in Figure 4a, ovarian cancer cells were stained with Annexin V-FITC conjugate after incubating with NCP-1/siRNAs for 24 h, indicating that the nanoparticles successfully induced cancer cell apoptosis. The presence of the characteristic DNA ladder in the NCP-1/siRNAs rather than NCP-1 indicated that co-delivery of cisplatin and pooled siRNA successfully induce cell apoptosis in cisplatin-resistant cells by silencing the MDR gene expression (Figure 4b). As shown in Figure S16 (SI), no apoptosis was observed in the Zn control group after a 24-h incubation by flow cytometry. Healthy cell percentages of NCP-1, NCP-1/si*Bcl-2*, NCP-1/si*P-gp*, NCP-1/*sisurvivin*, NCP-1/siRNAs, Zn control/siRNAs, and free cisplatin solution were determined to be 79.8%, 49.1%, 51.9%, 39.4%, 25.2%, 94.8%, and 67.0%, respectively, indicating that NCP-1/siRNAs was the most potent in inducing apoptosis (Figure 4c, Figure S16, Table S2, SI). Additionally, NCP-1/siRNAs evoked no immunogenic response in Raw 264.7 macrophage and SKOV-3 cells (Figure S17, SI), indicating the lack of immuno-toxicity of NCP-1/siRNAs.

### 2.6. Anticancer efficacy in SKOV-3 xenografts

Local delivery of chemotherapeutic drugs is an efficient strategy for achieving high drug doses at the target site while minimizing systemic exposure. Encouraged by significantly enhanced *in vitro* anticancer efficacy, we evaluated the *in vivo* antitumor effect of NCP-1/siRNAs in cisplatin-resistant SKOV-3 subcutaneous xenografts. As depicted in Figure 5, no antitumor efficacy was observed for free cisplatin (1 mg/kg dose) plus free pooled siRNAs (0.25 mg/kg dose), NCP-1 (1 mg/kg dose), and Zn control/siRNAs (0.25 mg/kg dose), of which the *P* values were 0.8311, 0.1502, 0.8594 compared to control by two-tail T-test, respectively. In contrast, NCP-1/siRNAs at the same cisplatin and/or siRNA doses exhibited remarkable tumor regression; the average tumor size decreased from 97±6 to 38±20 $mm^3$ ($P$=0.0010 vs. control). Compared to the control group, the mRNA expression levels of Bcl-2, survivin, and P-gp in the tumors of mice receiving local injection of NCP-1/siRNAs were significantly reduced by 58.8%, 51.7%, and 48.7%, respectively (Figure S18). Accordingly, the Bcl-2, P-gp, and survivin protein production of tumors treated with NCP-1/siRNAs were down-regulated by 74%, 48%, and 84%, respectively, in comparison to the control (Figure 5d). The significant knockdown of Bcl-2, P-gp, and survivin in the tumor site presumably sensitized the tumor cells towards cisplatin treatment, leading to the much enhanced antitumor effect by the co-delivery of cisplatin and siRNAs. The TUNEL assay showed that the fluorescence intensity of DNA fragmentation and the relative percentage of

apoptotic cells in the NCP-1/siRNAs group were higher than those in the other groups, indicating their superior anticancer efficacy (Figure 5c & d).

No significant body weight loss or immunogenic response was observed after repeated treatment with NCP-1/siRNAs (Figure S19 – S20, SI). We also performed histological analysis of the kidneys, livers, spleens, and lungs of mice treated with NCP-1/siRNAs. No cast formation, swelling, desquamation, tubular damage or microvillus disappearance was noted in the kidney, indicating that NCP-1/siRNAs would not induce nephrotoxicity which is a major concern of cisplatin toxicity (Figure S21). In addition, NCP-1/siRNAs treatment did not induce haemorrhages or dystrophy of hepatocytes in liver, increase the number of lymphoid follicles in spleen, or cause inflammatory cell infiltration in lungs (Figure S21). These results suggested the safety of NCP-1/siRNAs when applied *in vivo*.

## 4. Conclusions

We have reported the first effort of utilizing self-assembled nanoscale coordination polymers as an efficient vehicle to simultaneously deliver cisplatin and pooled siRNAs to cisplatin-resistant ovarian cancer cells. Our results demonstrated that NCP-1/siRNAs could mediate effective gene silencing in cisplatin-resistant ovarian cancer cells to overcome MDR and re-sensitize the cells to cisplatin treatment. Consequently, the co-delivery of cisplatin and pooled siRNAs drastically enhanced the *in vivo* chemotherapeutic effects in cisplatin-resistant SKOV-3 ovarian cancer mouse model. The versatility of the NCP delivery platform should allow its further optimization for potential clinical translation to treat late stage, resistant cancers.

## Supplementary Material

Refer to Web version on PubMed Central for supplementary material.

## Acknowledgments

We thank NIH (UO1-CA151455) for funding support. We thank C. Poon for the assistance in ICP-MS analysis and Shirley Bond and Dr. Vytas Bindokas from the Integrated Microscopy Core Facility at the University of Chicago for the help with CLSM analysis.

## References

1. Coleman RL, Monk BJ, Sood AK, Herzog TJ. Latest research and treatment of advanced-stage epithelial ovarian cancer. Nat Rev Clin Oncol. 2013; 10:211–224. [PubMed: 23381004]
2. Vaughan S, Coward JI, Bast RC, Berchuck A, Berek JS, Brenton JD, et al. Rethinking ovarian cancer: recommendations for improving outcomes. Nature Reviews Cancer. 2011; 11:719–725.
3. Roberts D, Schick J, Conway S, Biade S, Laub PB, Stevenson JP, et al. Identification of genes associated with platinum drug sensitivity and resistance in human ovarian cancer cells. Brit J Cancer. 2005; 92:1149–1158. [PubMed: 15726096]
4. Kelland L. The resurgence of platinum-based cancer chemotherapy. Nat Rev Cancer. 2007; 7:573–584. [PubMed: 17625587]
5. Lowery WJ, Lowery AW, Barnett JC, Lopez-Acevedo M, Lee PS, Secord AA, et al. Cost-effectiveness of early palliative care intervention in recurrent platinum-resistant ovarian cancer. Gynecol Oncol. 2013; 130:426–430. [PubMed: 23769759]

6. Galluzzi L, Senovilla L, Vitale I, Michels J, Martins I, Kepp O, et al. Molecular mechanisms of cisplatin resistance. Oncogene. 2012; 31:1869–1883. [PubMed: 21892204]
7. Siddik ZH. Cisplatin: mode of cytotoxic action and molecular basis of resistance. Oncogene. 2003; 22:7265–7279. [PubMed: 14576837]
8. Kelland L. The resurgence of platinum-based cancer chemotherapy. Nat Rev Cancer. 2007; 7:573–584. [PubMed: 17625587]
9. Igney FH, Krammer PH. Death and anti-death: Tumour resistance to apoptosis. Nat Rev Cancer. 2002; 2:277–288. [PubMed: 12001989]
10. Holohan C, Van Schaeybroeck S, Longley DB, Johnston PG. Cancer drug resistance: an evolving paradigm. Nat Rev Cancer. 2013; 13:714–726. [PubMed: 24060863]
11. Yang Y, Hu YX, Wang YH, Li J, Liu F, Huang L. Nanoparticle Delivery of Pooled siRNA for Effective Treatment of Non-Small Cell Lung Caner. Mol Pharmaceut. 2012; 9:2280–2289.
12. Agarwal R, Kaye SB. Ovarian cancer: Strategies for overcoming resistance to chemotherapy. Nat Rev Cancer. 2003; 3:502–516. [PubMed: 12835670]
13. Herzog TJ. Recurrent ovarian cancer: How important is it to treat to disease progression? Clin Cancer Res. 2004; 10:7439–7449. [PubMed: 15569973]
14. Fire A, Xu SQ, Montgomery MK, Kostas SA, Driver SE, Mello CC. Potent and specific genetic interference by double-stranded RNA in Caenorhabditis elegans. Nature. 1998; 391:806–811. [PubMed: 9486653]
15. Giljohann DA, Seferos DS, Prigodich AE, Patel PC, Mirkin CA. Gene Regulation with Polyvalent siRNA-Nanoparticle Conjugates. J Am Chem Soc. 2009; 131:2072. -+ [PubMed: 19170493]
16. Xiong XB, Lavasanifar A. Traceable Multifunctional Micellar Nanocarriers for Cancer-Targeted Co-delivery of MDR-1 siRNA and Doxorubicin. Acs Nano. 2011; 5:5202–5213. [PubMed: 21627074]
17. Patel NR, Pattni BS, Abouzeid AH, Torchilin VP. Nanopreparations to overcome multidrug resistance in cancer. Adv Drug Deliver Rev. 2013; 65:1748–1762.
18. Johnstone RW, Ruefli AA, Lowe SW. Apoptosis: A link between cancer genetics and chemotherapy. Cell. 2002; 108:153–164. [PubMed: 11832206]
19. Reed JC, Miyashita T, Takayama S, Wang HG, Sato T, Krajewski S, et al. BCL-2 family proteins: Regulators of cell death involved in the pathogenesis of cancer and resistance to therapy. J Cell Biochem. 1996; 60:23–32. [PubMed: 8825412]
20. Pennati M, Folini M, Zaffaroni N. Targeting survivin in cancer therapy: fulfilled promises and open questions. Carcinogenesis. 2007; 28:1133–1139. [PubMed: 17341657]
21. Zaffaroni N, Daidone MG. Survivin expression and resistance to anticancer treatments: perspectives for new therapeutic interventions. Drug Resist Update. 2002; 5:65–72.
22. Ambudkar SV, Kimchi-Sarfaty C, Sauna ZE, Gottesman MM. P-glycoprotein: from genomics to mechanism. Oncogene. 2003; 22:7468–7485. [PubMed: 14576852]
23. Ziegler S, Pries V, Hedberg C, Waldmann H. Target Identification for Small Bioactive Molecules: Finding the Needle in the Haystack. Angew Chem Int Edit. 2013; 52:2744–2792.
24. Cho YS, Lee GY, Sajja HK, Qian WP, Cao ZH, He WL, et al. Targeted Delivery of siRNA-Generating DNA Nanocassettes Using Multifunctional Nanoparticles. Small. 2013; 9:1964–1973. [PubMed: 23292656]
25. Oberoi HS, Nukolova NV, Kabanov AV, Bronich TK. Nanocarriers for delivery of platinum anticancer drugs. Adv Drug Deliver Rev. 2013; 65:1667–1685.
26. Davis ME, Chen Z, Shin DM. Nanoparticle therapeutics: an emerging treatment modality for cancer. Nat Rev Drug Discov. 2008; 7:771–782. [PubMed: 18758474]
27. Petros RA, DeSimone JM. Strategies in the design of nanoparticles for therapeutic applications. Nat Rev Drug Discov. 2010; 9:615–627. [PubMed: 20616808]
28. Ling D, Park W, Park SJ, Lu Y, Kim KS, Hackett MJ, et al. Multifunctional Tumor pH-Sensitive Self-Assembled Nanoparticles for Bimodal Imaging and Treatment of Resistant Heterogeneous Tumors. J Am Chem Soc. 2014

29. Sun TWY, Wang Y, Xu J, Zhao X, Vangveravong S, Mach RH, Xia Y. Using SV119-Gold Nanocage Conjugates to Eradicate Cancer Stem Cells Through a Combination of Photothermal and Chemo Therapies. Advanced healthcare materials. 2014
30. Lee GY, Qian WP, Wang LY, Wang YA, Staley CA, Satpathy M, et al. Theranostic Nanoparticles with Controlled Release of Gemcitabine for Targeted Therapy and MRI of Pancreatic Cancer. Acs Nano. 2013; 7:2078–2089. [PubMed: 23402593]
31. Lee JH, Kim JW, Cheon J. Magnetic nanoparticles for multi-imaging and drug delivery. Mol Cells. 2013; 35:274–284. [PubMed: 23579479]
32. Zhuang J, Kuo CH, Chou LY, Liu DY, Weerapana E, Tsung CK. Optimized Metal-Organic-Framework Nanospheres for Drug Delivery: Evaluation of Small-Molecule Encapsulation. Acs Nano. 2014; 8:2812–2819. [PubMed: 24506773]
33. Lee JE, Lee N, Kim H, Kim J, Choi SH, Kim JH, et al. Uniform Mesoporous Dye-Doped Silica Nanoparticles Decorated with Multiple Magnetite Nanocrystals for Simultaneous Enhanced Magnetic Resonance Imaging, Fluorescence Imaging, and Drug Delivery. J Am Chem Soc. 2010; 132:552–527. [PubMed: 20017538]
34. Gomes-da-Silva LC, Fonseca NA, Moura V, de Lima MCP, Simoes S, Moreira JN. Lipid-Based Nanoparticles for siRNA Delivery in Cancer Therapy: Paradigms and Challenges. Accounts Chem Res. 2012; 45:1163–1171.
35. Lin Q, Jin CS, Huang H, Ding L, Zhang Z, Chen J, et al. Nanoparticle-Enabled, Image-Guided Treatment Planning of Target Specific RNAi Therapeutics in an Orthotopic Prostate Cancer Model. Small. 2014
36. Cutler JI, Auyeung E, Mirkin CA. Spherical Nucleic Acids. J Am Chem Soc. 2012; 134:1376–1391. [PubMed: 22229439]
37. Zheng D, Giljohann DA, Chen DL, Massich MD, Wang XQ, Iordanov H, et al. Topical delivery of siRNA-based spherical nucleic acid nanoparticle conjugates for gene regulation. P Natl Acad Sci USA. 2012; 109:11975–11980.
38. Taratula O, Garbuzenko O, Savla R, Wang YA, He HX, Minko T. Multifunctional Nanomedicine Platform for Cancer Specific Delivery of siRNA by Superparamagnetic Iron Oxide Nanoparticles-Dendrimer Complexes. Curr Drug Deliv. 2011; 8:59–69. [PubMed: 21034421]
39. Macfarlane RJ, Lee B, Jones MR, Harris N, Schatz GC, Mirkin CA. Nanoparticle Superlattice Engineering with DNA. Science. 2011; 334:204–208. [PubMed: 21998382]
40. Xu XY, Xie K, Zhang XQ, Pridgen EM, Park GY, Cui DS, et al. Enhancing tumor cell response to chemotherapy through nanoparticle-mediated codelivery of siRNA and cisplatin prodrug. P Natl Acad Sci USA. 2013; 110:18638–18643.
41. Bhirde AA, Patel V, Gavard J, Zhang GF, Sousa AA, Masedunskas A, et al. Targeted Killing of Cancer Cells in Vivo and in Vitro with EGF-Directed Carbon Nanotube-Based Drug Delivery. Acs Nano. 2009; 3:307–316. [PubMed: 19236065]
42. Mangala LS, Zuzel V, Schmandt R, Leshane ES, Haider JB, Armaiz-Pena GN, et al. Therapeutic Targeting of ATP7B in Ovarian Carcinoma. Clin Cancer Res. 2009; 15:3770–3780. [PubMed: 19470734]
43. Liu DPC, Lu K, He C, Lin W. Self-assembled nanoscale coordination polymers with trigger release properties for effective anticancer therapy. Nature Commnications. 2014
44. Rieter WJ, Pott KM, Taylor KML, Lin WB. Nanoscale coordination polymers for platinum-based anticancer drug delivery. J Am Chem Soc. 2008; 130:11584. -+ [PubMed: 18686947]
45. Taylor-Pashow KML, Della Rocca J, Xie ZG, Tran S, Lin WB. Postsynthetic Modifications of Iron-Carboxylate Nanoscale Metal-Organic Frameworks for Imaging and Drug Delivery. J Am Chem Soc. 2009; 131:14261. -+ [PubMed: 19807179]
46. Huxford-Phillips RC, Russell SR, Liu DM, Lin WB. Lipid-coated nanoscale coordination polymers for targeted cisplatin delivery. Rsc Adv. 2013; 3:14438–14443. [PubMed: 24058727]
47. Huxford RC, deKrafft KE, Boyle WS, Liu DM, Lin WB. Lipid-coated nanoscale coordination polymers for targeted delivery of antifolates to cancer cells. Chem Sci. 2012; 3:198–204.
48. Liu DM, Kramer SA, Huxford-Phillips RC, Wang SZ, Della Rocca J, Lin WB. Coercing bisphosphonates to kill cancer cells with nanoscale coordination polymers. Chem Commun. 2012; 48:2668–2670.

49. Whitehead KA, Langer R, Anderson DG. Knocking down barriers: advances in siRNA delivery. Nat Rev Drug Discov. 2009; 8:129–138. [PubMed: 19180106]
50. Jiang S, Eltoukhy AA, Love KT, Langer R, Anderson DG. Lipidoid-Coated Iron Oxide Nanoparticles for Efficient DNA and siRNA delivery. Nano Letters. 2013; 13:1059–1064. [PubMed: 23394319]
51. Kulkarni A, DeFrees K, Hyun SH, Thompson DH. Pendant Polymer:Amino-beta-Cyclodextrin:siRNA Guest:Host Nanoparticles as Efficient Vectors for Gene Silencing. J Am Chem Soc. 2012; 134:7596–7599. [PubMed: 22545899]
52. Lee SJ, Huh MS, Lee SY, Min S, Lee S, Koo H, et al. Tumor-Homing Poly-siRNA/Glycol Chitosan Self-Cross-Linked Nanoparticles for Systemic siRNA Delivery in Cancer Treatment. Angew Chem Int Edit. 2012; 51:7203–7207.
53. Takemoto H, Miyata K, Hattori S, Ishii T, Suma T, Uchida S, et al. Acidic pH-Responsive siRNA Conjugate for Reversible Carrier Stability and Accelerated Endosomal Escape with Reduced IFN alpha-Associated Immune Response. Angew Chem Int Edit. 2013; 52:6218–6221.
54. Kunjachan S, Rychlik B, Storm G, Kiessling F, Lammers T. Multidrug resistance: Physiological principles and nanomedical solutions. Adv Drug Deliver Rev. 2013; 65:1852–1865.
55. Biswas S, Deshpande PP, Navarro G, Dodwadkar NS, Torchilin VP. Lipid modified triblock PAMAM-based nanocarriers for siRNA drug co-delivery. Biomaterials. 2013; 34:1289–1301. [PubMed: 23137395]
56. Lengyel E, Burdette JE, Kenny HA, Matei D, Pilrose J, Haluska P, et al. Epithelial ovarian cancer experimental models. Oncogene. 2014; 33:3619–3633. [PubMed: 23934194]

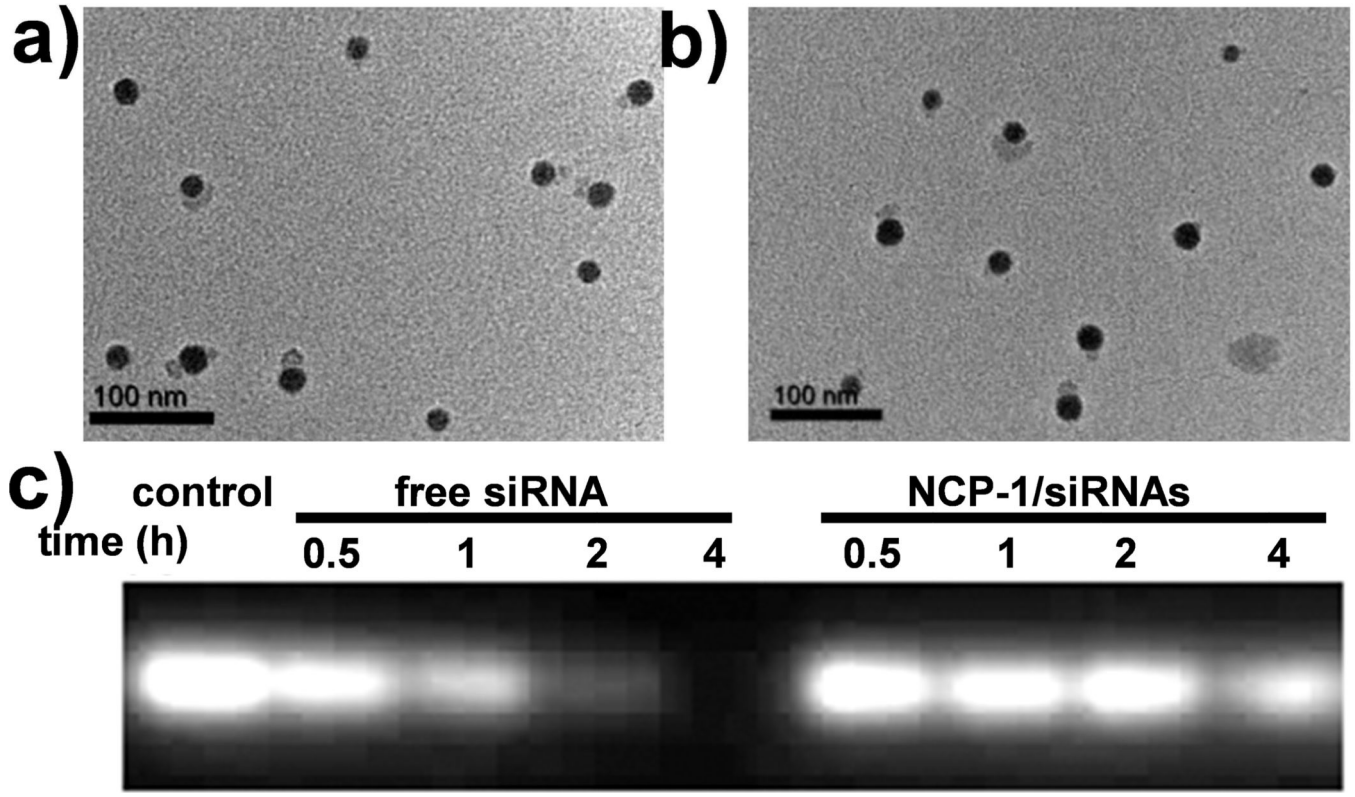


**Figure 1.**

TEM images of NCP-1 coated with DOTAP (a) and NCP-1/siRNAs (b) showing the spherical, mono-dispersed, and well-defined morphology. (c) Enhanced serum stability of siRNAs that were loaded into NCP-1 as evaluated by electrophoresis.

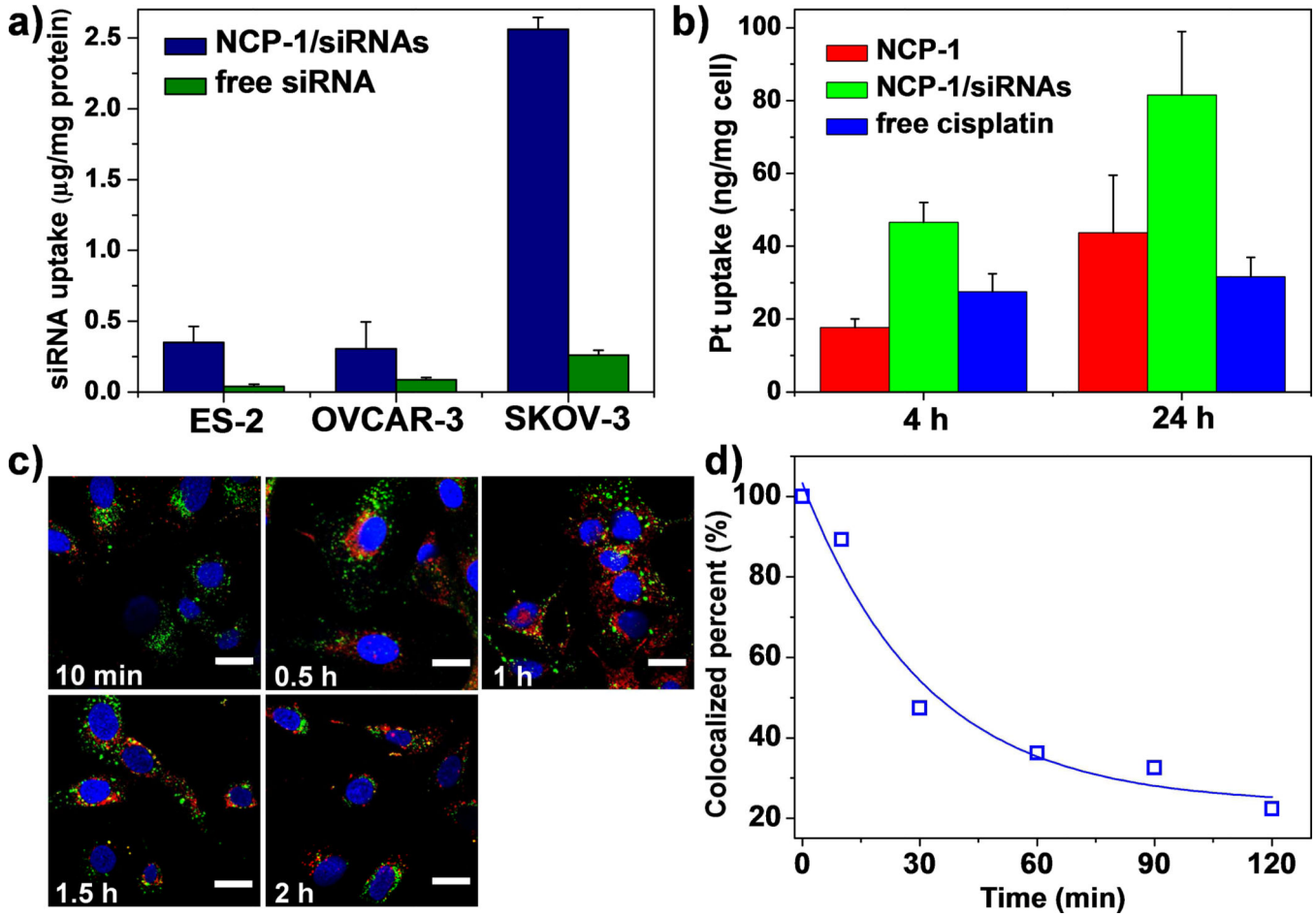


**Figure 2.**

(a) Cellular uptake amount of siRNA in ovarian cancer cells after incubating for 4 h (n=3). (b) Cellular uptake amount of Pt in SKOV-3 cells after incubating for 4 h and 24 h (n=3). (c) Time-dependent endosomal escape of NCP-1/siRNAs (TAMRA-labeled, red fluorescence) in SKOV-3 cells. Endosome/lysosome and nuclei were stained with Lysotracker Green and DAPI, respectively. Bar represented 20 μm. (d) Percent co-localization of siRNA and endosome/lysosome quantified by Image J based on (c).

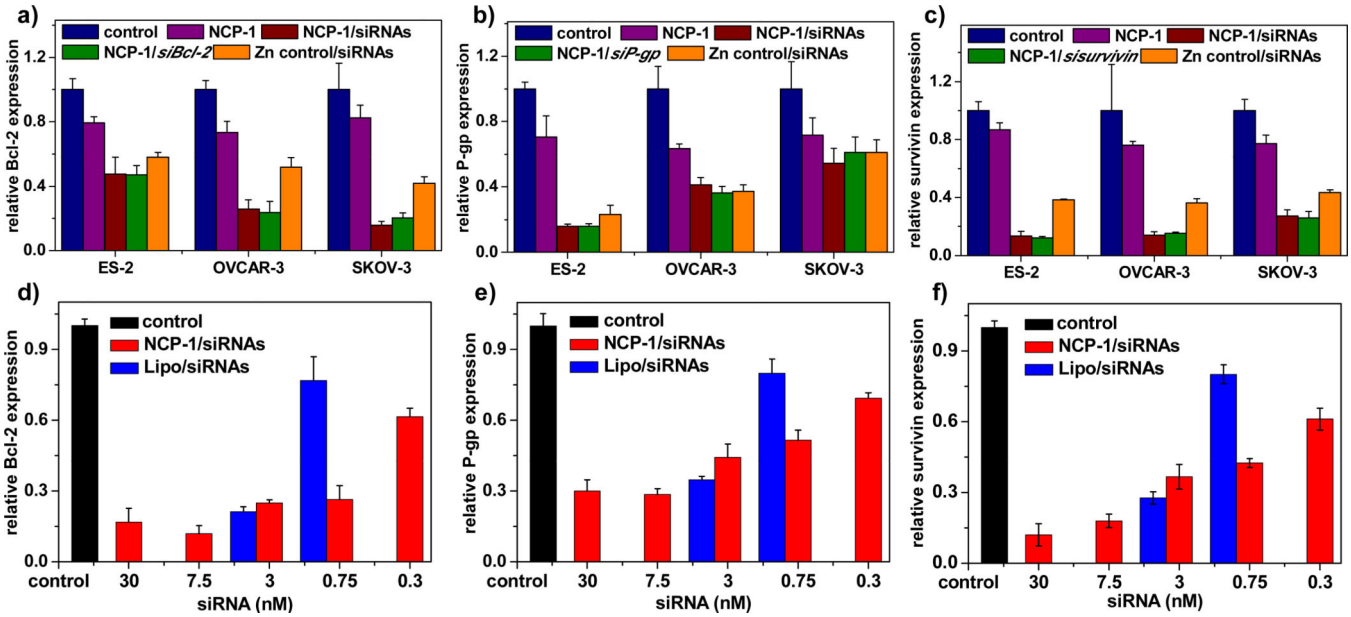


**Figure 3.**

Survivin (a), Bcl-2 (b), and P-gp (c) relative expression levels in ovarian cancer cells transfected with NCP-1, NCP-1/siRNAs, NCP-1/si*survivin*, NCP-1/si*Bcl-2*, NCP-1/si*P-gp*, and Zn control/siRNAs at an siRNA concentration of 30 nM (n=3). (d)-(f) Dose-dependent transfection efficiency mediated by NCP-1/siRNAs and Lipofecatamine RNAiMAX/siRNAs (Lipo/siRNAs) in SKOV-3 cells (n=3).

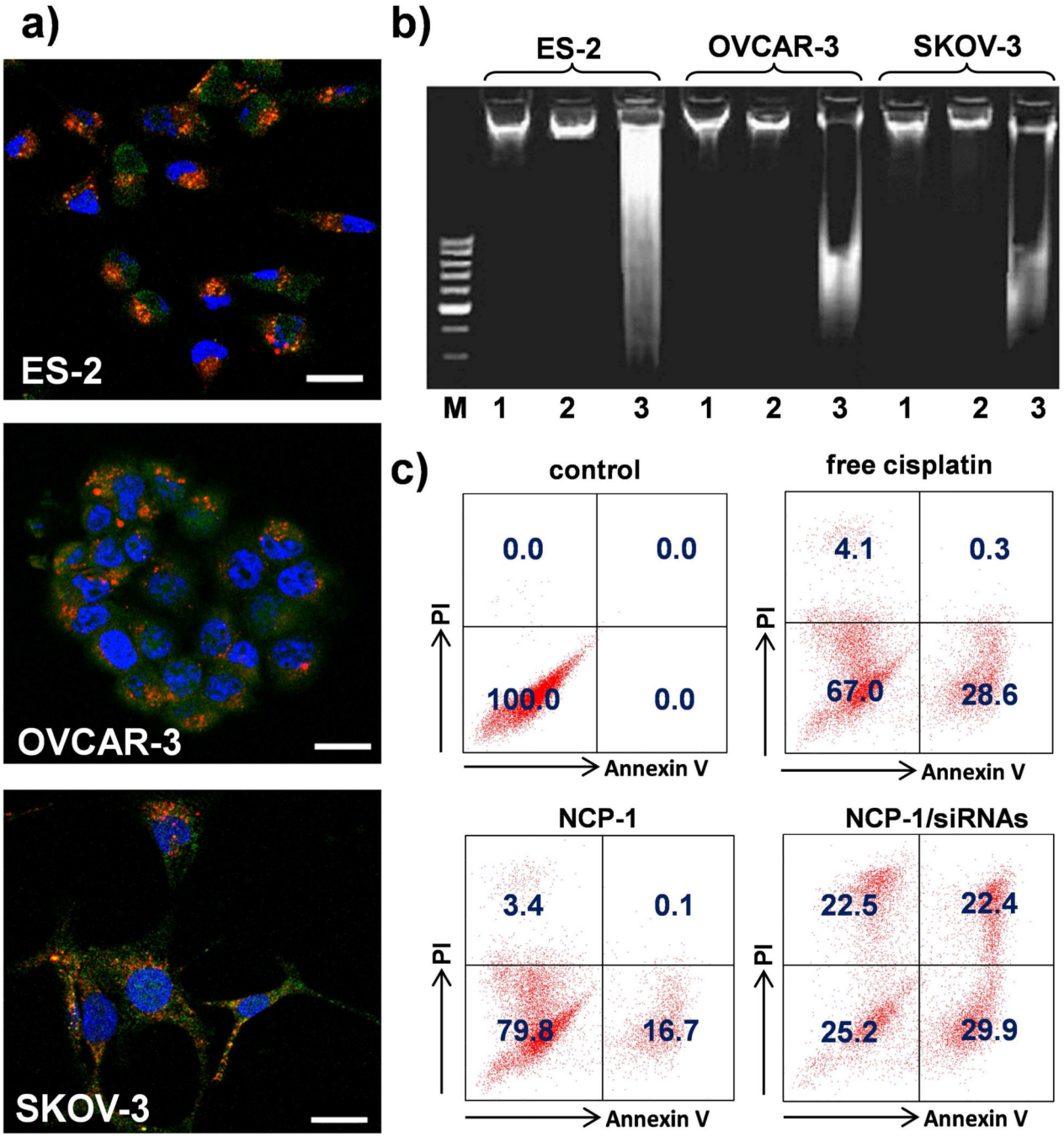


**Figure 4.**

(a) CLSM images showing cell apoptosis and siRNA internalization in ES-2, OVCAR-3, and SKOV-3 cells after incubation with NCP-1/siRNAs for 24 h. The siRNA was labeled with TAMRA (red fluorescence).The cells were stained with Annexin V FITC Conjugate and the nuclei were stained with DAPI. Bar represented 20 μm. (b) Analysis of DNA ladder on 2% (w/v) agarose gel at 35 V for 5 h after DNA extraction from the ovarian cancers treated with NCP-1 or NCP-1/siRNA. M: DNA marker; 1: control; 2: NCP-1; 3: NCP-1/siRNAs. (c) Annexin V/PI analysis of SKOV-3 cells after the incubation with saline

(control), NCP-1, NCP-1/siRNAs and free cisplatin for 24 h. The quadrants from lower left to upper left (counter clockwise) represent healthy, early apoptotic, late apoptotic, and necrotic cells, respectively. The percentage of cells in each quadrant was shown on the graphs.

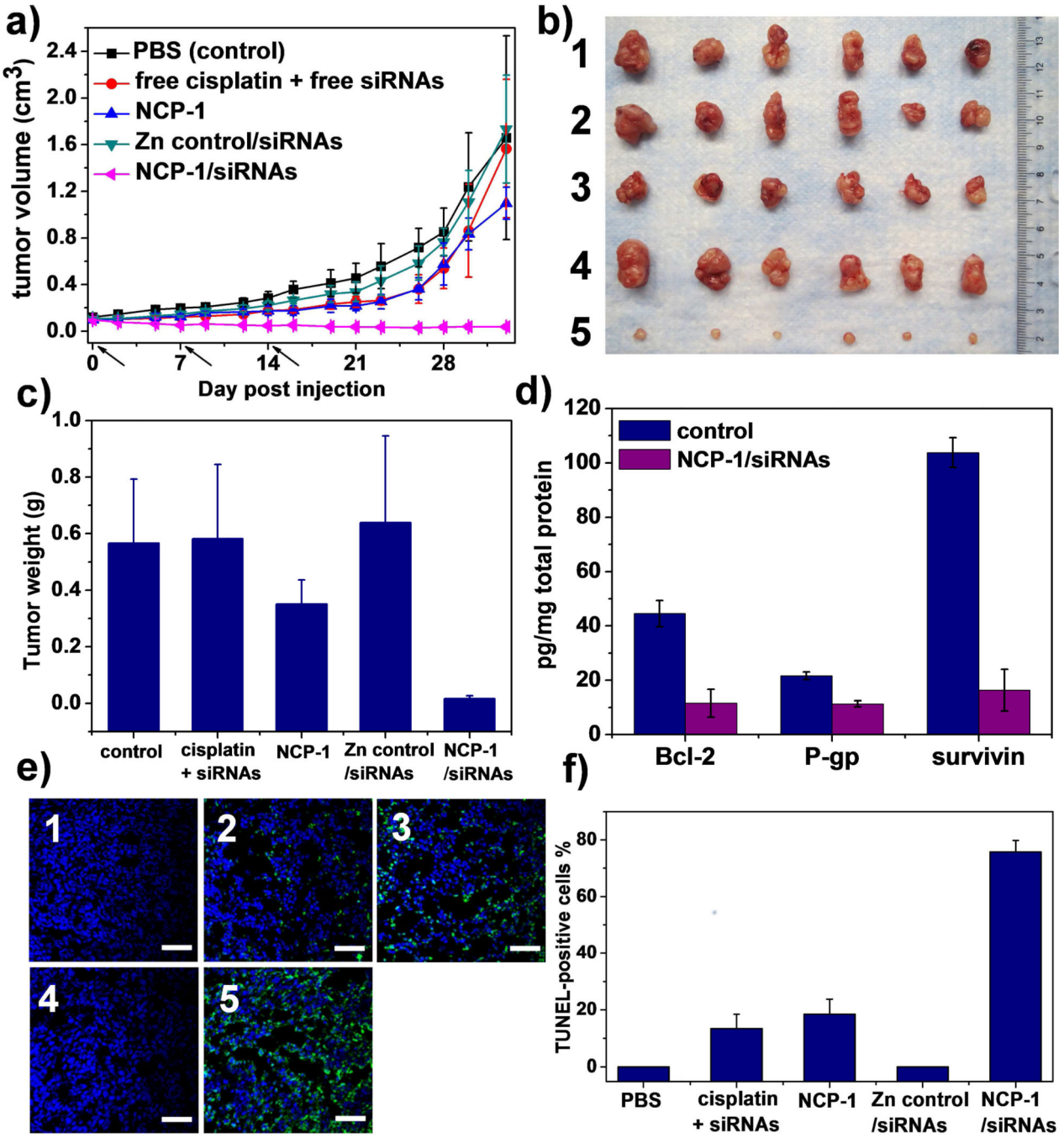


**Figure 5.**

*In vivo* anticancer effects of NCP-1/siRNAs on SKOV-3 subcutaneous xenograft murine models. (a) Tumor growth curves of the mice receiving intratumoral injections (n=6). (b) Photograph of the excised tumors on day 33. 1: control; 2: free cisplatin + free siRNAs; 3: NCP-1; 4: Zn control/siRNAs; 5: NCP-1/siRNAs. (c) Weights of the excised tumors on Day 33. Indicated values were mean ± SD (n=6). The P values of free cisplatin plus free siRNAs, NCP-1, Zn control/siRNAs, and NCP-1/siRNAs compared to control were 0.9159, 0.0538, 0.6493, and 0.0001, respectively, by two-tail T-test. (d) The protein expression levels of

Bcl-2, P-gp, and survivin significantly decreased in the tumors of mice receiving intratumoral injection of NCP-1/siRNAs (n=3). The P values of NCP-1/siRNAs compared to control were 0.0012, 0.0006, and 0.00009 for Bcl-2, P-gp, and survivin expression, respectively, by two-tail T-test. (e) Representative CLSM images of TUNEL assays of tumor tissues. DNA fragment in apoptotic cells was stained with fluorescein-conjugated deoxynucleotides (green) and the nuclei were stained with DAPI (blue). 1: control; 2: free cisplatin + free siRNAs; 3: NCP-1; 4: Zn control/siRNAs; 5: NCP-1/siRNAs. Bar represented 50 μm. (f) The percentage of TUNEL-positive cells in tumor tissues (n=3).

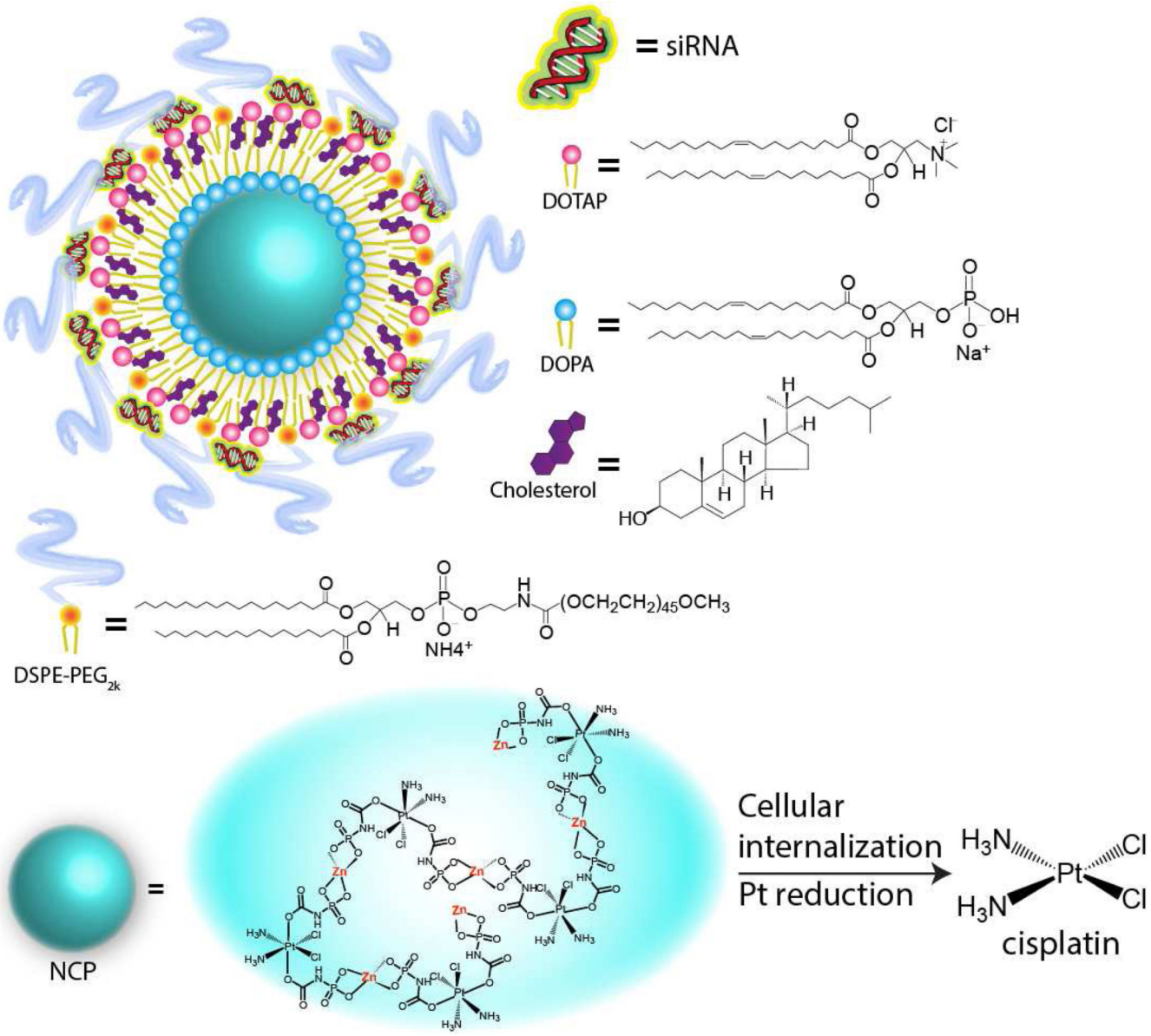


**Scheme 1.**

Schematic showing the compositions of NCP-1/siRNAs. Upon entering cancer cells, the intracellular reducing environment will trigger the cisplatin release via reductive degradation of NCP-1.

**Table 1**

Cisplatin $IC_{50}$ (μM) in ES-2, OVCAR-3, SKOV-3, A2780 and A2780/CDDP cells after a 72-h incubation.

| | ES-2 | OVCAR-3 | SKOV-3 | A2780 | A2780/CDDP |
|---|---|---|---|---|---|
| Free cisplatin | 37.6±1.9 | 44.4±3.2 | 59.5±1.2 | 4.4±1.0 | 24.0±3.1 |
| NCP-1 | 37.9± 0.4 | 50.7±0.9 | 56.0±2.2 | 3.3±0.4 | 23.7±5.6 |
| NCP-1/si*Bcl-2* | 25.4±1.2 | 28.8±2.1 | 25.9±0.6 | - | - |
| NCP-1 */siP-gp* | 14.6±1.1 | 39.2±1.1 | 44.4±3.4 | - | - |
| NCP-1 */sisurvivin* | 31.8±2.6 | 45.6±2.1 | 2.6±0.6 | - | - |
| NCP-1/siRNAs | 0.4±0.1 | 6.8±1.1 | 0.4±0.1 | 3.5±0.3 | 1.5±0.4 |